Mineralogy and Petrology (2021) 115:595–609
https://doi.org/10.1007/s00710-021-00749-9

ORIGINAL PAPER

# Brattforsite, $Mn_{19}(AsO_3)_{12}Cl_2$, a new arsenite mineral related to magnussonite, from Brattforsgruvan, Nordmark, Värmland, Sweden

Dan Holtstam[1] · Cristian Biagioni[2] · Ulf Hålenius[1]

Received: 21 December 2020 / Accepted: 31 March 2021 / Published online: 26 May 2021


## Abstract

Brattforsite is an approved mineral (IMA2019-127), with ideal formula $Mn_{19}(AsO_3)_{12}Cl_2$. Associated minerals in the type specimen from the Brattfors mine, Nordmark (Värmland, Sweden) include jacobsite, alleghanyite, phlogopite, calcite and dolomite. Brattforsite, forming subhedral, mostly equant crystals up to 0.5 mm across, is orange to reddish-brown with a white streak, and translucent with a resinous to vitreous lustre. The fracture is uneven to subconchoidal, and no cleavage is observed. It is very weakly pleochroic in yellow, optically biaxial (–) with $2V = 44(5)°$ and has calculated mean refractive index of 1.981. Measured and calculated density values are 4.49(1) and 4.54(1) $g{\cdot}cm^{-3}$, respectively. Chemical analyses yields (in wt%): MgO 0.62, CaO 1.26, MnO 48.66, FeO 0.13, $As_2O_3$ 46.72, Cl 2.61, $H_2O_{calc}$ 0.07, O ≡ Cl –0.59, sum 99.49, corresponding to the empirical formula $(Mn_{17.67}Ca_{0.58}Mg_{0.40}Fe_{0.05})_{\sum 18.70}As_{12.17}O_{35.90}Cl_{1.90}(OH)_{0.20}$, based on 38 (O + Cl + OH) atoms per formula unit. The five strongest Bragg peaks in the powder X-ray diffraction pattern are [*d* (Å), *I* (%), (*hkl*)]: 2.843,100, ($\overline{4}$ 44); 2.828, 99, (444); 1.731, 32, (880); 2.448, 28, (800); 1.739, 25, (088). Brattforsite is monoclinic and pseudotetragonal, space group *I*2/*a*, with unit-cell parameters $a = 19.5806(7)$, $b = 19.5763(7)$, $c = 19.7595(7)$ Å, $\beta = 90.393(3)°$, $V = 7573.9(5)$ Å$^3$ and $Z = 8$. The crystal structure was solved and refined to an $R_1$ index of 3.4 % for 7445 reflections [$F_o > 4\sigma(F_o)$]. Brattforsite has the same overall structural topology as magnussonite (i.e., the species can be considered as homeotypic), but with 12 independent tetrahedrally coordinated As sites and 21 Mn sites with varying (4–8) coordination. The Mn-centered polyhedra, bonded through edge- and face-sharing, give rise to a three-dimensional framework. The $(AsO_3)^{3-}$ groups are bonded to this framework through corner- and edge-sharing. Spectroscopic measurements (optical absorption, Raman, FTIR) carried out support the interpretation of the compositional and structural data.

**Keywords** Brattforsite · New mineral · Magnussonite · Arsenite · Skarn · Nordmark · Sweden

## Introduction

Arsenites form a subclass of rare, but significantly diverse, minerals with about 20 known species. They are most commonly characterized by the isolated $(AsO_3)^{3-}$ anion in their crystal structures, and typically formed during the late-stage evolution of Mn or base-metal polymetallic ores (Majzlan et al. 2014). Here we describe a recently approved arsenite mineral from Brattforsgruvan, Filipstad municipality, Värmland, Sweden, named brattforsite (IMA2019-127). The mineral has been the subject to previous studies, and was long considered a variety of magnussonite, a presumed cubic arsenite mineral, first described by Gabrielson (1956) from the Långban deposit (also in Filipstad, Värmland), with the current IMA-formula $Mn_{10}As_6O_{18}(OH,Cl)_2$ (Pasero 2021). Moore (1970a) found that the mineral from Brattforsgruvan was pseudocubic, with a tetragonal unit cell, $a = 19.58(2)$, $c = 19.72(2)$ Å, space group $I4_1/amd$. Dunn and Ramik (1984) noted a high Cl content of 2.7-3.0 wt% for the same mineral, and obtained the provisional formula $Mn_{10}As_6O_{18}Cl(OH)$.

Editorial handling: M. A.T.M. Broekmans

✉ Dan Holtstam
dan.holtstam@nrm.se

[1] Department of Geosciences, Swedish Museum of Natural History, Box 50007, SE-104 05 Stockholm, Sweden

[2] Dipartimento di Scienze della Terra, Università di Pisa, Via Santa Maria 53, I-56126 Pisa, Italy

The mineral name is given for the type locality, the mine Brattforsgruvan. This name was previously used informally, on a label to the type specimen, and mentioned by Paul B. Moore in a letter from 1967 (F.E. Wickman file, Archives of the Royal Swedish Academy of Sciences, Stockholm). "Brattfors" is the name of a neighbouring parish, and of an old iron smelter. Brattforsite corresponds to UM1984-09 in the list of valid unnamed mineral species (Smith and Nickel 2007). The holotype specimen is deposited in the type mineral collection of the Department of Geosciences, Swedish Museum of Natural History, Box 50007, SE-10405 Stockholm, Sweden, under collection number GEO-NRM 19100303. The single crystal used for X-ray diffraction intensity data measurement (a part of the holotype) is kept in the mineralogical collection of the Natural History Museum of Pisa University, under catalogue number 19912.

## Occurrence and paragenesis

Brattforsgruvan (59°49.99' N, 14°7.41' E, 230 m above shoreline) belongs to the Nordmark ore field (Nordmarks odalfält), which comprises about twenty old, small mines and prospects (Magnusson 1929). The principal ore mineral was magnetite, but a few of the old mines intersect enclaves with Mn oxides (dominantly hausmannite) and associated skarns, including Mn-bearing silicates and a number of exotic As-, Sb-, and B-oxyminerals (e.g., Sjögren 1884; Holtstam and Langhof 1995; Holtstam et al. 1998; Cooper et al. 2018). This particular mineralisation is related to the Långban-type of deposits in the Paleoproterozoic Bergslagen ore region (Moore 1970b). The ores and skarns of the Nordmark field are closely associated to a marble (dolomite-calcite) body adjacent to felsic metavolcanic rocks (Björck 1986). The Långban-type carbonate-hosted deposits primordially formed as Fe-Mn-Pb-As-Sb-rich precipitates from volcanogenic hydrothermal solutions in a shallow submarine environment at ca. 1.9 Ga (Boström et al. 1979; Holtstam and Mansfeld 2001). Subsequent regional metamorphism, deformation and intrusive events have affected the synvolcanic-synsedimentary protoliths until ca. 1.75 Ga (Stephens et al. 2009). Peak metamorphic conditions are estimated as $T$ = 600–650°C and $P$ = 0.3–0.4 GPa (Sandström and Holtstam 1999; Christy and Gatedal 2005).

The original occurrence of the present sample in the mine is unknown; it was purchased by the Swedish Museum of Natural History from Olof Backelin, a mining foreman and local mineral collector, in 1910. Backelin is noted as the source for two other type mineral specimens from this mine, katoptrite (Flink 1917) and manganhumite (Moore 1978). The mines of the Nordmark field closed in 1962 and are now inaccessible.

Arsenite minerals are typically confined to late-stage mineralization in fissures and druses in Långban-type deposits (Nysten et al. 1999); in the present case, it is probable that the new mineral has replaced a Mn-rich precursor mineral in the skarn mass, from alteration by a late- or post-metamorphic, As- and Cl-bearing fluid. Slightly reducing conditions in these rocks are indicated by the presence of manganosite and alabandite, observed in minor amounts in similar skarn matrices. Brattforsite occurs as crystals forming aggregates up to 8 mm across, in a granular matrix of (Fig. 1) jacobsite, calcite, dolomite, phlogopite and alleghanyite. Minor associated minerals identified by energy-dispersion microanalysis are rhodochrosite and johnbaumite. Subrounded grains of jacobsite commonly appear as inclusions in brattforsite. A Mn-As-(OH) mineral, tentatively identified as allactite, occurs filling fine fractures of brattforsite. Allactite is a late-stage vein mineral in the Mn mineralizations at Nordmark (Sjögren 1884).

## Physical and optical properties

Individual crystals of brattforsite are somewhat irregular in shape but essentially equant, and up to 0.5 mm in size. The macroscopic colour is orange to reddish brown, with a white streak. It has a vitreous to resinous lustre. Brattforsite is translucent and transparent in thin section. No fluorescence effects were detected in ultra-violet light. The hardness (Mohs) is estimated to 3–4. Neither an obvious cleavage nor parting is observed. Brattforsite is brittle and shows an uneven to subconchoidal fracture. Moore (1970a) reported 4.49 $g \cdot cm^{-3}$ for the density; a calculated value of 4.54(1) $g \cdot cm^{-3}$ is obtained for the ideal formula and unit-cell volume from single-crystal X-ray diffraction data. The mineral dissolves in 30 % hydrochloric acid at room temperature.

The refractive indices were not measured conventionally, because found higher than available reference liquids (> 1.8); the average calculated $n$ is 1.981 from Gladstone-Dale constants (Mandarino 1981). The mineral is optically biaxial (–),

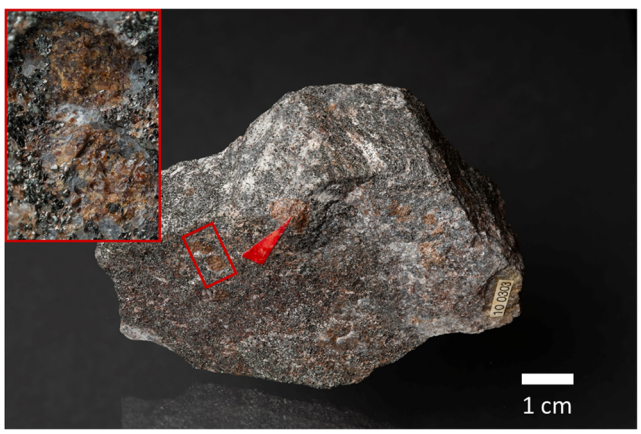


**Fig. 1** Image of the brattforsite (arrow points to the largest aggregate) type specimen with jacobsite (black) and calcite (whitish), GEO-NRM #19100303. Inset image shows a detail on the specimen (red frame). Photos: Torbjörn Lorin

with $2V_{meas} = 44(5)°$. The estimated birefringence is small, ~0.002. The dispersion is weak, with $v > r$. Brattforsite is very weakly pleochroic, in yellow hues. Polysynthetic twinning has been observed in a couple of grains. The angle of extinction between twin lamellae, up to 80 μm wide, is 27(1)°.

## Mineral chemistry

The mineral was mounted in epoxy resin and polished prior to analysis. Electron probe microanalysis (EPMA) was performed with a Cameca Camebax SX-50 instrument, running at 20 kV, with the sample current 12 nA, spot size = 2 μm and a take-off angle of 40°. Corrections of the raw data were executed with Cameca's PAP-routine, a modified ZAF procedure (Pouchou and Pichoir 1984). Used reference materials and the results from four spot analyses are given in Table 1. The concentration values for CuO and ZnO were below or close to the detection limit. Minor $(OH)^-$ in the crystal structure is indicated by infrared spectra (see the following). The empirical formula for brattforsite, calculated on the basis of 38 (O + Cl + OH) atoms per formula unit (*apfu*), with As as a trivalent cation, is $(Mn_{17.67}Ca_{0.58}Mg_{0.40}Fe_{0.05})_{\Sigma 18.70}As_{12.17}O_{35.90}Cl_{1.90}(OH)_{0.20}$. The simplified formula may be written (Mn, Ca, Mg, Fe)$_{19}$As$_{12}$O$_{36}$(Cl, OH)$_2$ and the ideal formula is $Mn_{19}As_{12}O_{36}Cl_2$ or $Mn_{19}(AsO_3)_{12}Cl_2$, which corresponds to (in wt%) MnO 52.04, $As_2O_3$ 45.84, Cl 2.74, O ≡ Cl -0.62, total 100.00.

## Infra-red, Raman and optical absorption spectroscopy

### Infrared spectroscopy

Fourier-transform infrared (FTIR) spectra were measured on a double-side polished single crystal (thickness = 116 μm) using a Bruker Vertex spectrometer equipped with a Hyperion II microscope, a Globar source, a $CaF_2$ beam-splitter, and an InSb detector. Data were acquired during 64 scans in the wavenumber range 2000–12,000 $cm^{-1}$ at a spectral resolution of 4 $cm^{-1}$. No absorption bands apart from very weak ones in the OH stretching region (Fig. 2) were observed. From comparison with the intensity of OH stretching bands in the infrared spectrum of a magnussonite single crystal (Fig. 2) from the holotype specimen GEO-NRM #g32215, the $H_2O$-concentration in the brattforsite crystal is estimated to be ≤ 0.07 wt %, corresponding to ≤ 0.2 OH *apfu*. A relative low energy, with initial absorption at ca. 2700 $cm^{-1}$, and a broadness of the envelope of the bands marking OH stretching modes may be due to relatively strong hydrogen bonding in magnussonite and in brattforsite. Alternatively, these features are due to OH stretching bands superimposed on an absorption band caused by a low-energy *d-d* transition in a transition metal cation as e.g. $Fe^{2+}$.

**Table 1** Chemical data (in wt%) for brattforsite

| Constituent | Mean | Range | Stand. dev. (2σ) | Reference material |
|---|---|---|---|---|
| MgO | 0.62 | 0.53–0.73 | 0.08 | MgO |
| CaO | 1.26 | 1.26–1.27 | 0.01 | $CaSiO_3$ |
| MnO | 48.66 | 48.33–48.99 | 0.26 | $MnTiO_3$ |
| FeO | 0.13 | 0.08–0.18 | 0.04 | $Fe_2O_3$ |
| $As_2O_3$ | 46.72 | 46.15–47.17 | 0.43 | GaAs |
| Cl | 2.61 | 2.57–2.66 | 0.03 | Vanadinite |
| $H_2O$* | 0.07 | | | |
| O≡Cl | -0.59 | | | |
| | 99.48 | | | |

*$H_2O$ content estimated from FTIR spectrum

### Micro-Raman spectroscopy

A Raman spectrum of brattforsite (Fig. 3) was collected from a randomly oriented, polished crystal fragment on a LabRAM HR 800 micro-spectrometer, using a 514 nm Ar-ion laser source at < 1 mW power, a Peltier-cooled (–70 °C) 1024 × 256 pixel CCD detector (Synapse), an Olympus M Plan N 100×/0.9 NA objective and laser spot of ca. 3 μm. A 600 grooves/cm grating was used, and the resolution is about 1 $cm^{-1}$. Spectral positions were corrected against the Raman band at 789 $cm^{-1}$ of a SiC-6*H* crystal measured on {0001}. Instrument control and data acquisition (range 50-4000 $cm^{-1}$, 10 s exposure time in 20 cycles) were made with the *LabSpec 5* software. No laser-induced degradation of the sample was observed. A sample of magnussonite (type specimen) was measured for a comparison (Fig. 3).

The spectra were found to be featureless in the range 4000–1000 $cm^{-1}$; prominent Raman peaks are identified for brattforsite at 786, 760 (shoulder), 708, 660, 510, 203 and 117 $cm^{-1}$ (Fig. 3). The most intense band at 786 $cm^{-1}$ is ascribed to symmetric stretching of the $(AsO_3)^{3-}$ groups and the shoulder at 760 $cm^{-1}$ to antisymmetric stretching (cf. Frost and Bahfenne 2010). The corresponding bands in magnussonite are found at 811 and 794 $cm^{-1}$. The peaks between 700 and 500 $cm^{-1}$, including minor ones, for both minerals are resulting either from stretching vibrations of $Mn^{2+}$-O(Cl,OH) bonds or from bending vibrations of $(AsO_3)^{3-}$. Specifically, the band at 510 $cm^{-1}$ is consistent with octahedrally coordinated $Mn^{2+}$, whereas the one at 660 $cm^{-1}$ would be compatible with lower coordination numbers for this cation (Bernardini et al. 2021). Peaks in the low-frequency region from ca. 200 $cm^{-1}$ are probably related to lattice modes.

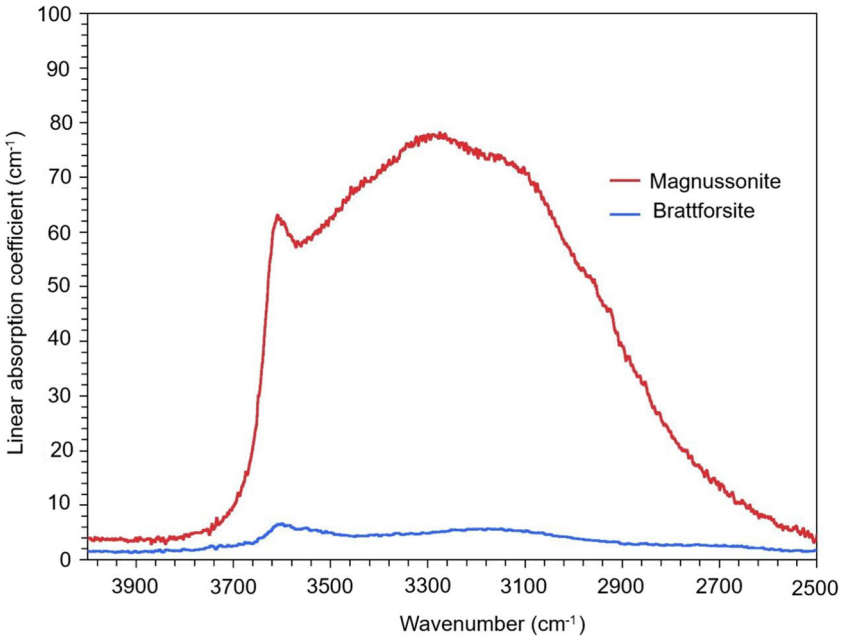


**Fig. 2** FTIR spectra of brattforsite (blue line) and holotype magnussonite (red line) in the OH-stretching region

## Optical absorption spectroscopy

Polarized optical absorption spectra (Fig. 4) were measured on two double-side polished oriented crystal sections (one *XZ* and one *YZ* section), both 70 μm thick, of brattforsite. The crystals were oriented by means of optical microscopy. The spectra were recorded in the range 10,000–32,000 $cm^{-1}$ with an AVASPEC-ULS2048 × 16 spectrometer attached via a 400-μm UV fibre cable to a Zeiss Axiotron UV-microscope. A 75 W Xenon arc lamp served as a light source and Zeiss Ultrafluar 10× lenses were used as objective and condenser. The size of the circular measure aperture was 64 μm in diameter. An UV-quality Glan-Thompson prism with a working range from 250 to 2700 nm (40,000 to 3704 $cm^{-1}$) was used as polarizer. The recorded spectra show a set of absorption bands caused by spin-forbidden electronic *d-d* transitions in $Mn^{2+}$ superimposed on an UV absorption edge. The most prominent of these bands, at 23,650 $cm^{-1}$, marks the field independent $^6A_1(S) \rightarrow {}^4A_1{}^4E(G)$ transition in $Mn^{2+}$. The calculated molar absorption coefficient (ε) of the band is approximately 1 $l \cdot mole^{-1} \cdot cm^{-1}$, which is comparable to the ε-value recorded for the corresponding band in spectra of magnussonite (Hålenius and Lindqvist 1996). An additional, broad and strongly polarized band at ~13,700 $cm^{-1}$ is tentatively assigned to a spin-allowed *d-d* transition in $Fe^{2+}$ in four-fold coordination or in a strongly axial distorted octahedral

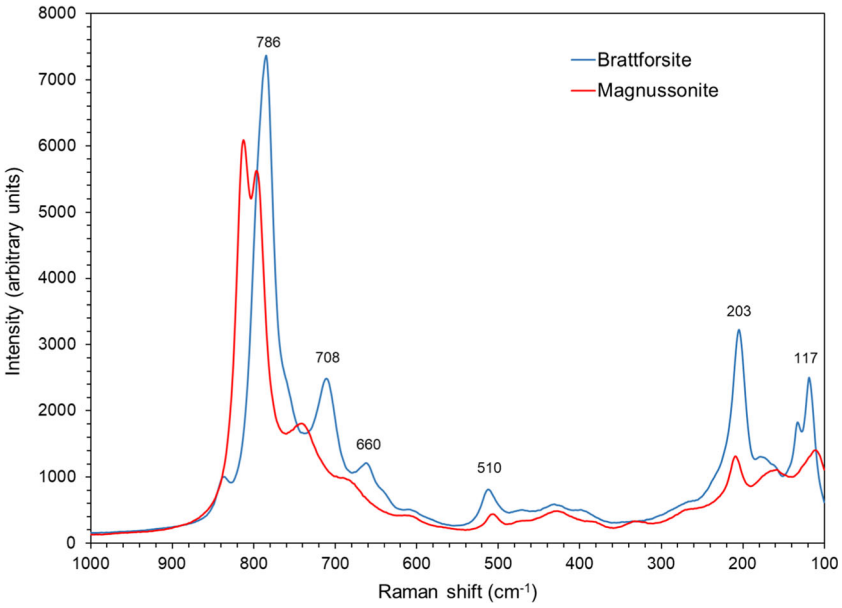


**Fig. 3** Raman spectra of brattforsite and holotype magnussonite (GEO-NRM #g32215) recorded using a 514-nm laser

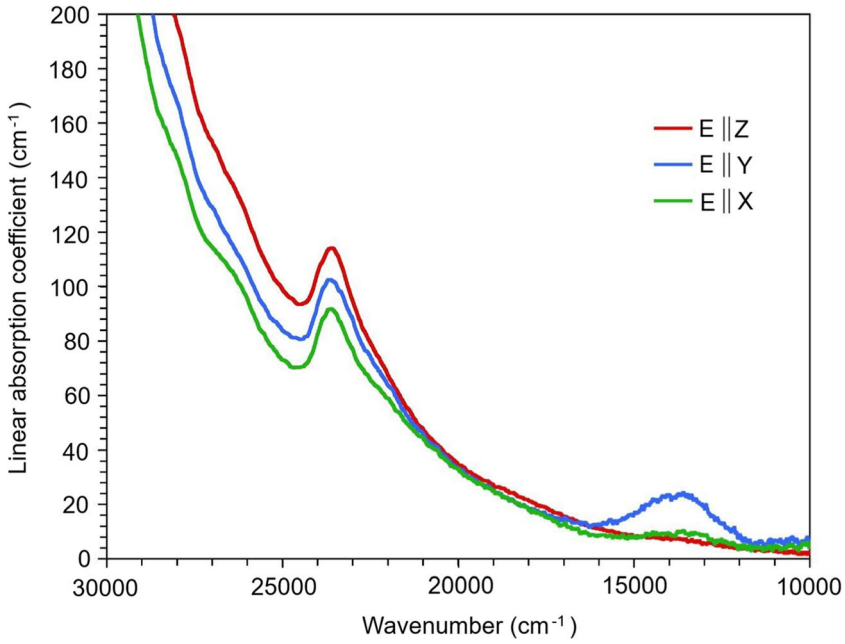


**Fig. 4** Polarized optical absorption spectra of brattforsite

coordination. Based on the molar absorption coefficient (~ 165 l·mole$^{-1}$·cm$^{-1}$) of a corresponding absorption band at ~ 15,300 cm$^{-1}$ in spectra of magnussonite (Hålenius and Lindqvist 1996), the FeO concentration in brattforsite is calculated at 0.15 wt%, which compares well with a concentration of 0.13 wt% determined by EPMA (Table 1).

## X-ray crystallography

X-ray powder diffraction data were collected with a PANalytical X'Pert$^3$ powder diffractometer equipped with an X'celerator silicon-strip detector and operated at 40 mA and 45 kV (Cu$K\alpha$-radiation, $\lambda = 1.5406$ Å). Bragg-peak positions (Table 2) were determined with the *PANalytical HighScore Plus 4.6* software and corrected against an external Si standard (NBS 640b). The monoclinic (space group *I*2/*a*, #15) unit-cell parameters refined by a least-squares method from the powder data are: $a = 19.592(2)$ Å, $b = 19.586(2)$ Å, $c = 19.770(2)$ Å, $\beta = 90.413(7)°$ and $V = 7586(1)$ Å$^3$ for $Z = 8$.

Single-crystal X-ray intensity data were collected using a Bruker Smart Breeze diffractometer equipped with a Photon II CCD detector and graphite monochromatized Mo$K\alpha$ radiation. The detector-to-crystal working distance was set at 50 mm. Data were collected using ω scan mode in 0.5° slices, with an exposure time of 20 s per frame. Correction for Lorentz and polarization factors, absorption, and background were applied using the package of software *Apex*3 (Bruker AXS Inc. 2016). Brattforsite is monoclinic, with unit-cell parameters $a = 27.7223(9)$, $b = 19.5763(7)$, $c = 19.5806(7)$ Å, $\beta = 134.5410(10)°$, $V = 7573.9(5)$ Å$^3$. The statistical tests on the distribution of $|E|$ values ($|E^2 - 1| = 1.006$) indicated the occurrence of an inversion center. The examination of systematic absences suggested the space group symmetry *C*2/*c*. The crystal structure of brattforsite was solved in this space group through direct methods using *Shelxs*-97 and refined using *Shelxl*-2018 (Sheldrick 2015). Following the recommendation of Mighell (2003), the *C*-centered monoclinic cell was transformed in a conventional *I*-centered cell, through the matrix [0 0–1 | 0 1 0 | 1 0 1], obtaining the pseudotetragonal unit-cell parameters $a = 19.5806(7)$, $b = 19.5763(7)$, $c = 19.7595(7)$ Å, $\beta = 90.393(3)°$, $V = 7573.9(5)$ Å$^3$, space group *I*2/*a*. These unit-cell parameters can be compared with those reported by Moore (1970a), $a = 19.58(2)$, $c = 19.72(2)$ Å, space group $I4_1/amd$. The following neutral scattering curves, taken from the *International Tables for Crystallography* (Wilson 1992), were used: Mn vs. Ca at Mn sites, As at As sites, O at O sites, and Cl vs. O at Cl sites. Several Mn sites were found fully occupied by Mn and their site occupancy factors (s.o.f.) were fixed to the full occupancy by Mn. The anisotropic structural model of brattforsite converged to $R_1 = 0.0343$ for 7445 reflections with $F_o > 4\sigma(F_o)$ and 640 refined parameters. A crystallographic information file (CIF) is available as electronic supplementary material. Details of data collection and refinement are given in Table 3. Fractional atom coordinates and displacement parameters are reported in Table 4, whereas Table 5 contains interatomic distances and bond-valence sums (BVS) for cation sites, and Table 6 the BVS sums for the anion sites. BVS were calculated using the bond parameters of Gagné and Hawthorne (2015) for As–O, Ca–O, and Mn–O bonds, and those of Brese and O'Keeffe (1991) for Mn–Cl and Ca–Cl bonds.

**Table 2** X-ray powder diffraction data ($d$ in Å) for brattforsite

| $I$ | $d_{obs}$ | $d_{calc}$ | $h$ | $k$ | $l$ |
|---|---|---|---|---|---|
| 4 | 8.023 | 8.030 | -2 | 1 | 1 |
| 1 | 6.963 | 6.957 | 0 | 2 | 2 |
| 1 | 5.259 | 5.254 | 1 | 2 | 3 |
| 1 | 4.901 | 4.898 | 4 | 0 | 0 |
| 1 | 4.178 | 4.175 | 3 | 3 | 2 |
| 10 | 4.011 | 4.013 | 2 | 2 | 4 |
| 1 | 3.572 | 3.573 | 5 | 1 | 2 |
| 3 | 3.462 | 3.463 | 4 | 4 | 0 |
| 4 | 3.205 | 3.202 | 1 | 1 | 6 |
| 3 | 3.176 | 3.178 | 1 | 6 | 1 |
| 6 | 3.124 | 3.123 | 0 | 2 | 6 |
| 14 | 3.097 | 3.097 | 2 | 6 | 0 |
| 100 | 2.843 | 2.843 | -4 | 4 | 4 |
| 99 | 2.828 | 2.829 | 4 | 4 | 4 |
| 8 | 2.676 | 2.677 | 3 | 3 | 6 |
| 7 | 2.667 | 2.666 | -1 | 7 | 2 |
| 5 | 2.490 | 2.490 | -6 | 5 | 1 |
| 16 | 2.471 | 2.471 | 0 | 0 | 8 |
| 28 | 2.448 | 2.449 | 8 | 0 | 0 |
| 9 | 2.348 | 2.348 | 3 | 5 | 6 |
| 2 | 2.277 | 2.277 | 4 | 7 | 3 |
| 2 | 2.0695 | 2.0708 | 1 | 8 | 5 |
| 3 | 1.9581 | 1.9586 | -1 | 1 | 10 |
| 6 | 1.9419 | 1.9423 | -7 | 7 | 2 |
| 6 | 1.9380 | 1.9384 | 7 | 7 | 2 |
| 4 | 1.8035 | 1.8027 | 3 | 10 | 3 |
| 16 | 1.7457 | 1.7460 | 8 | 0 | -8 |
| 25 | 1.7392 | 1.7393 | 0 | 8 | 8 |
| 32 | 1.7314 | 1.7315 | 8 | 8 | 0 |
| 6 | 1.6914 | 1.6914 | 7 | 9 | 2 |
| 5 | 1.6097 | 1.6100 | -1 | 7 | 10 |
| 6 | 1.6052 | 1.6046 | 5 | 5 | 10 |
| 6 | 1.6002 | 1.6000 | -7 | 10 | 1 |
| 4 | 1.5286 | 1.5281 | 3 | 6 | 11 |
| 10 | 1.4907 | 1.4907 | -4 | 4 | 12 |
| 11 | 1.4848 | 1.4847 | 4 | 4 | 12 |
| 15 | 1.4810 | 1.4810 | -12 | 4 | 4 |
| 16 | 1.4751 | 1.4751 | 12 | 4 | 4 |

## Crystal structure description

### General features

The crystal structure of brattforsite (Fig. 5) shows the occurrence of thirty-three independent cation sites (twelve As sites and twenty-one Mn-dominant sites) and thirty-eight anion positions.

The crystal structure can be described as formed by polyhedral layers stacked along **c**. Within a unit-cell, eight layers occur; three symmetrically distinct layers, labelled $L_0$, $L_1$, and $L_2$, alternate in the unit-cell according to the sequence shown in Fig. 5. Figure 6 shows each single layer as seen down **c**. The layer $L_0$ is formed by rows of Mn-centered polyhedra running along [110] and [-110]. These rows show the sequence ···Mn(2)-Mn(6)-Mn(13)-Mn(4)-Mn(3)-Mn(8)-Mn(13)-Mn(9)-Mn(2)···, with Mn(13) occurring at the intersection between perpendicular rows. The intersection of the rows form a square cavity where a trimer composed of Mn(7)-Mn(20)-Mn(5) occurs, along with ($AsO_3$) groups. Two As sites, i.e., As(1) and As(5), point in the + **c** direction, whereas As(4) and As(8) point in the –**c** direction. The layer $L_1$ shows clusters formed by four independent Mn sites, i.e., Mn(10), Mn(11), Mn(15), and Mn(16). This cluster forms chains along **a**, obtained through corner-sharing between Mn(15) and Mn(16) belonging to consecutive tetramers, and through ($AsO_3$) groups [As(2) and As(7)]. Along **b**, the connection between these chains is due to ($AsO_3$) groups [As(9) and As(12)]. The layer $L_2$ has two independent tetramers, formed by Mn(1), Mn(21), and two Mn(7) and by Mn(14), Mn(18), and two Mn(12), respectively. These clusters are bonded along **a** through As(10) and As(11), whereas along **b** the connection is due to the occurrence of As(3) and As(6).

Notwithstanding such a description, the large number of connections between Mn-centered polyhedra, bonded through edge- and face-sharing, give rise to a three-dimensional framework. The $(AsO_3)^{3-}$ groups are bonded to this three-dimensional framework through corner- and edge-sharing. They are located on the walls of the structural cavities, with their $4s^2$ lone-electron pairs pointing towards the center of the cavities.

### Atom coordination

Arsenic displays the typical asymmetric trigonal pyramidal coordination, showing < As–O > distances ranging between 1.764 and 1.793 Å, in agreement with the < As–ϕ > value of 1.782 Å reported by Majzlan et al. (2014). The BVS at these sites range between 2.88 and 3.08 valence units (v.u.), in agreement with the occurrence of $As^{3+}$.

Manganese, along with minor Ca, Mg, and Fe, shows coordination numbers ranging from four to eight. Ten sites show a variably distorted octahedral coordination; among them, $MnO_6$, $MnO_5Cl$ and $MnO_4Cl_2$ polyhedra can be recognized. $MnO_6$ octahedra have < Mn–O > distances ranging between 2.193 and 2.234 Å, with individual distances varying between 2.098 and 2.385 Å. Gagné and Hawthorne (2020) gave an average bond distance for six-fold coordinated $Mn^{2+}$ of 2.20(8) Å, in agreement with the observed values. BVS at these sites are in the range 1.89–2.07 v.u., thus agreeing with the occurrence of divalent cations, mainly represented by $Mn^{2+}$, with only a negligible substitution by $Ca^{2+}$. Two sites,

**Table 3** Crystal data and experimental conditions for brattforsite

| Crystal data | |
|---|---|
| Crystal size (mm) | 0.125×0.070×0.030 |
| Cell setting, space group | Monoclinic, *I*2/*a* |
| *a* (Å) | 19.5806(7) |
| *b* (Å) | 19.5763(7) |
| *c* (Å) | 19.7595(7) |
| β (°) | 90.393(3) |
| *V* (Å$^3$) | 7573.9(5) |
| *Z* | 8 |
| Data collection and refinement | |
| Radiation, wavelength (Å) | Mo *K*α, λ=0.71073 |
| Temperature (K) | 293 |
| $2\theta_{max}$ (°) | 55.00 |
| Measured reflections | 84,979 |
| Unique reflections | 8686 |
| Reflections with $F_o > 4\sigma(F_o)$ | 7445 |
| $R_{int}$ | 0.0550 |
| *R*σ | 0.0271 |
| Range of *h*, *k*, *l* | −25≤*h*≤25, |
| | −25≤*k*≤25, |
| | −25≤*l*≤25 |
| *R* [$F_o > 4\sigma(F_o)$] | 0.0343 |
| *R* (all data) | 0.0440 |
| *wR* (on $F_o^2$) | 0.0698 |
| Goof | 1.081 |
| Number of least-squares parameters | 640 |
| Maximum and minimum residual peak (*e* Å$^{-3}$) | 1.37 [at 0.86 Å from Mn(20)] |
| | -1.50 [at 0.50 Å from Mn(17)] |

i.e., Mn(19) and Mn(20), are coordinated by five $O^{2-}$ anion and one $Cl^-$. Whereas the former has a pure Mn occupancy, the latter is a mixed (Mn,Ca) position, agreeing with an average bond distance larger than that shown by Mn(19). Both sites have a BVS of 1.92 v.u. Finally, the Mn(14) site displays four short bonds with $O^{2-}$ (average < Mn–O > = 2.102 Å) and two longer Mn–Cl distances (at ca. 2.94 Å). A six-fold coordination is assumed for four other Mn sites. Two of them, i.e., Mn(2) and Mn(3), have a distorted trigonal prismatic coordination, with bond distances ranging between 2.044 and 2.386 Å, and < Mn–O > distances of 2.219 and 2.229 Å. Their BVS are 1.92 and 2.00 v.u. Other two six-fold coordinated sites, Mn(10) and Mn(12), have a very distorted trigonal prismatic coordination, with five shorter bonds (< Mn–O > distances of 2.149 and 2.190 Å, respectively), and a longer one, at 2.914 and 2.657 Å, respectively. Indeed, the coordination of Mn(10) may be described as a [5 + 1] coordination, forming a distorted square pyramid. The < Mn–O > distance observed at Mn(10) is fully consistent with the average distance reported by Gagné and Hawthorne (2020) for five-fold coordinated $Mn^{2+}$, i.e., 2.14(5) Å. In addition, the range of observed bond distances for such a coordination, 2.024–2.267 Å (Gagné and Hawthorne 2020), agrees with the Mn–O distances observed for Mn(10). This is a bonding environment similar to that observed for Mn(7) and Mn(11); these sites can be described as square pyramids, with Mn–O distances ranging between 1.996 and 2.296 Å. For the Mn(11) site, the addition of a definitely longer bond at 3.098 Å increases the coordination number to six, allowing the description of this site as a very distorted trigonal prism; for the Mn(7), the sixth ligand is further away, at ~ 3.20 Å. The BVS at Mn(7), Mn(10), Mn(11), and Mn(12) are 2.02, 1.94, 1.92, and 1.87 v.u., respectively.

Mn(13) and Mn(15) show a seven-fold coordination. The former has six short bonds, ranging between 2.153 and 2.366 Å. A longer bond at 2.905 Å increases its coordination number to seven. Additionally, another O atom is located at 3.111 Å from Mn(13). Similarly, Mn(15) has six short bonds, varying between 2.187 and 2.437 Å, and a seventh one at 2.714 Å. Both these sites show a very minor Ca content, and their BVS are 1.81 and 1.82 v.u., respectively. These relatively low BVS

**Table 4** Atom sites, Wyckoff position, site occupancy factors (*s.o.f.*), fractional atomic coordinates, and equivalent isotropic displacement parameters ($Å^2$) for brattforsite

| Site | *Wyckoff position* | *s.o.f.* | *x/a* | *y/b* | *z/c* | $U_{eq}$ |
|---|---|---|---|---|---|---|
| As(1) | 8*f* | $As_{1.00}$ | 0.00026(3) | 0.00384(3) | 0.36526(3) | 0.00759(11) |
| As(2) | 8*f* | $As_{1.00}$ | 0.26751(3) | 0.38362(3) | 0.24917(3) | 0.00779(11) |
| As(3) | 8*f* | $As_{1.00}$ | 0.13233(3) | 0.48762(3) | -0.00286(3) | 0.00709(11) |
| As(4) | 8*f* | $As_{1.00}$ | -0.23774(3) | 0.75188(3) | 0.62083(3) | 0.00915(11) |
| As(5) | 8*f* | $As_{1.00}$ | -0.00584(3) | 0.48915(3) | 0.37206(3) | 0.00885(11) |
| As(6) | 8*f* | $As_{1.00}$ | 0.36796(3) | 0.51262(3) | 0.50022(3) | 0.00888(11) |
| As(7) | 8*f* | $As_{1.00}$ | 0.25747(3) | 0.61840(3) | 0.25161(3) | 0.00713(11) |
| As(8) | 8*f* | $As_{1.00}$ | 0.24865(3) | 0.75318(3) | 0.11621(3) | 0.00878(11) |
| As(9) | 8*f* | $As_{1.00}$ | 0.11763(3) | 0.24611(3) | 0.23714(3) | 0.00862(11) |
| As(10) | 8*f* | $As_{1.00}$ | -0.00448(3) | 0.63314(3) | -0.00611(3) | 0.00668(11) |
| As(11) | 8*f* | $As_{1.00}$ | 0.00119(3) | 0.62936(3) | 0.48024(3) | 0.00980(11) |
| As(12) | 8*f* | $As_{1.00}$ | -0.12020(3) | 0.25240(3) | 0.24160(3) | 0.00967(11) |
| Mn(1) | 4*e* | $Mn_{0.98(2)}Ca_{0.02(2)}$ | ¼ | 0.38327(6) | 0 | 0.0093(4) |
| Mn(2) | 8*f* | $Mn_{1.00}$ | 0.26853(4) | 0.48476(4) | 0.12663(4) | 0.01023(17) |
| Mn(3) | 8*f* | $Mn_{1.00}$ | 0.26618(4) | 0.51994(4) | 0.37702(4) | 0.00989(17) |
| Mn(4) | 8*f* | $Mn_{1.00}$ | 0.12676(4) | 0.61359(4) | 0.36013(4) | 0.01110(17) |
| Mn(5) | 8*f* | $Mn_{1.00}$ | 0.10589(4) | 0.36064(4) | -0.12841(4) | 0.00956(17) |
| Mn(6) | 8*f* | $Mn_{1.00}$ | -0.13415(4) | -0.11411(4) | 0.36738(4) | 0.00918(17) |
| Mn(7) | 8*f* | $Mn_{1.00}$ | -0.13997(4) | 0.75787(5) | 0.47466(4) | 0.01251(18) |
| Mn(8) | 8*f* | $Mn_{1.00}$ | 0.36147(4) | 0.38206(4) | 0.38759(4) | 0.01182(17) |
| Mn(9) | 8*f* | $Mn_{0.95(1)}Ca_{0.05(1)}$ | 0.13329(4) | 0.62053(4) | -0.11775(4) | 0.0080(3) |
| Mn(10) | 8*f* | $Mn_{1.00}$ | 0.01231(4) | 0.11482(5) | 0.21872(4) | 0.01449(18) |
| Mn(11) | 8*f* | $Mn_{1.00}$ | -0.00514(4) | 0.38023(4) | 0.23258(4) | 0.01210(17) |
| Mn(12) | 8*f* | $Mn_{1.00}$ | 0.12484(4) | 0.75883(4) | -0.02179(4) | 0.01246(18) |
| Mn(13) | 8*f* | $Mn_{0.98(2)}Ca_{0.02(2)}$ | -0.00476(4) | 0.75914(5) | 0.37537(4) | 0.0126(3) |
| Mn(14) | 4*e* | $Mn_{1.00}$ | ¼ | 0.62067(7) | 0 | 0.0212(3) |
| Mn(15) | 8*f* | $Mn_{0.99(2)}Ca_{0.01(2)}$ | 0.12888(4) | -0.00782(4) | 0.24386(4) | 0.0120(3) |
| Mn(16)a | 8*f* | $Mn_{0.93(1)}$ | 0.13067(5) | 0.48605(6) | 0.26213(6) | 0.0121(4) |
| Mg(16)b | 8*f* | $Mg_{0.07(1)}$ | 0.1285(15) | 0.512(2) | 0.236(2) | 0.0121(4) |
| Mn(17) | 8*f* | $Mn_{1.00}$ | -0.11231(5) | 0.35349(5) | 0.37999(4) | 0.01533(19) |
| Mn(18) | 4*e* | $Mn_{0.62(2)}Ca_{0.38(2)}$ | ¼ | 0.86777(7) | 0 | 0.0109(4) |
| Mn(19) | *8f* | $Mn_{1.00}$ | -0.04792(5) | 0.17255(5) | 0.34637(4) | 0.01620(19) |
| Mn(20) | 8*f* | $Mn_{0.59(2)}Ca_{0.41(2)}$ | -0.05565(7) | 0.71124(6) | 0.60384(6) | 0.0297(4) |
| Mn(21)a | 4*e* | $Mn_{0.16(2)}$ | ¼ | 0.379(3) | ½ | 0.018(3) |
| Mn(21)b | 8*f* | $Mn_{0.84(2)}$ | 0.2378(17) | 0.3810(2) | 0.4864(19) | 0.018(3) |
| O(1) | 8*f* | $O_{1.00}$ | 0.0816(2) | 0.1879(2) | 0.1766(2) | 0.0172(9) |
| O(2) | 8*f* | $O_{1.00}$ | -0.06842(19) | 0.6698(2) | -0.06039(19) | 0.0113(8) |
| O(3) | 8*f* | $O_{1.00}$ | 0.01289(19) | 0.08228(19) | 0.32077(19) | 0.0116(8) |
| O(4) | 8*f* | $O_{1.00}$ | -0.28296(19) | 0.68937(19) | 0.5720(2) | 0.0133(8) |
| O(5) | 8*f* | $O_{1.00}$ | 0.15984(19) | 0.42065(19) | -0.05812(19) | 0.0112(8) |
| O(6) | 8*f* | $O_{1.00}$ | -0.0740(2) | 0.30780(19) | 0.18649(19) | 0.0120(8) |
| O(7) | 8*f* | $O_{1.00}$ | 0.0739(2) | 0.31688(19) | 0.20207(19) | 0.0122(8) |
| O(8) | 8*f* | $O_{1.00}$ | 0.20299(18) | 0.43146(199 | 0.20602(18) | 0.0091(8) |
| O(9) | 8*f* | $O_{1.00}$ | 0.29368(19) | 0.5676(2) | 0.18713(18) | 0.0106(8) |
| O(10) | 8*f* | $O_{1.00}$ | 0.3204(2) | 0.5405(2) | 0.5695(2) | 0.0194(9) |
| O(11) | 8*f* | $O_{1.00}$ | 0.3365(2) | 0.5758(2) | 0.4449(2) | 0.0198(10) |
| O(12) | 8*f* | $O_{1.00}$ | 0.2909(2) | 0.4364(2) | 0.31783(19) | 0.0133(8) |
| O(13) | 8*f* | $O_{1.00}$ | 0.29332(19) | 0.68950(19) | 0.06905(19) | 0.0106(8) |

**Table 4** (continued)

| Site | *Wyckoff position* | *s.o.f.* | *x/a* | *y/b* | *z/c* | $U_{eq}$ |
|---|---|---|---|---|---|---|
| O(14) | 8*f* | $O_{1.00}$ | 0.3079(2) | 0.8175(2) | 0.09011(19) | 0.0126(8) |
| O(15) | 8*f* | $O_{1.00}$ | 0.32274(19) | 0.5936(2) | 0.31008(18) | 0.0117(8) |
| O(16) | 8*f* | $O_{1.00}$ | 0.06195(19) | 0.6767(2) | -0.04714(19) | 0.0120(8) |
| O(17) | 8*f* | $O_{1.00}$ | -0.16007(19) | 0.7651(2) | 0.57589(19) | 0.0120(8) |
| O(18) | 8*f* | $O_{1.00}$ | 0.0662(2) | 0.2220(2) | 0.3064(2) | 0.0173(9) |
| O(19) | 8*f* | $O_{1.00}$ | 0.18681(18) | 0.45740(19) | 0.06274(18) | 0.0091(7) |
| O(20) | 8*f* | $O_{1.00}$ | -0.0723(2) | 0.5438(2) | 0.3393(2) | 0.0160(9) |
| O(21) | 8*f* | $O_{1.00}$ | -0.0792(2) | 0.2715(2) | 0.3192(2) | 0.0165(9) |
| O(22) | 8*f* | $O_{1.00}$ | -0.0774(2) | 0.1739(2) | 0.2291(2) | 0.0169(9) |
| O(23) | 8*f* | $O_{1.00}$ | -0.0766(2) | 0.6733(2) | 0.4714(2) | 0.0224(10) |
| O(24) | 8*f* | $O_{1.00}$ | 0.0495(2) | 0.6735(2) | 0.4179(2) | 0.0239(10) |
| O(25) | 8*f* | $O_{1.00}$ | 0.0329(3) | 0.6740(2) | 0.5507(3) | 0.0372(14) |
| O(26) | 8*f* | $O_{1.00}$ | -0.0312(3) | 0.4192(3) | 0.3221(3) | 0.0441(16) |
| O(27) | 8*f* | $O_{1.00}$ | -0.28715(19) | 0.81942(19) | 0.58221(19) | 0.0108(8) |
| O(28) | 8*f* | $O_{1.00}$ | 0.05617(19) | 0.53422(19) | 0.32215(19) | 0.0114(8) |
| O(29) | 8*f* | $O_{1.00}$ | 0.33408(19) | 0.4160(2) | 0.19755(19) | 0.0132(8) |
| O(30) | 8*f* | $O_{1.00}$ | 0.19618(19) | 0.5643(2) | 0.28994(18) | 0.0107(8) |
| O(31) | 8*f* | $O_{1.00}$ | 0.3167(2) | 0.4481(2) | 0.46106(19) | 0.0131(8) |
| O(32) | 8*f* | $O_{1.00}$ | 0.18253(19) | 0.54978(19) | -0.04530(18) | 0.0093(8) |
| O(33) | 8*f* | $O_{1.00}$ | -0.06395(18) | -0.04036(19) | 0.31823(19) | 0.0105(8) |
| O(34) | 8*f* | $O_{1.00}$ | 0.06720(19) | -0.04516(19) | 0.32800(19) | 0.0108(8) |
| O(35) | 8*f* | $O_{1.00}$ | 0.1831(2) | 0.7824(2) | 0.06114(19) | 0.0129(8) |
| O(36) | 8*f* | $O_{1.00}$ | -0.01984(19) | 0.6828(2) | 0.06788(18) | 0.0111(8) |
| Cl(1) | 8*f* | $Cl_{0.94(1)}(OH)_{0.06(1)}$ | -0.14573(8) | 0.11429(9) | 0.39393(9) | 0.0265(7) |
| Cl(2) | 8*f* | $Cl_{0.95(2)}(OH)_{0.05(2)}$ | -0.13190(12) | 0.61224(10) | 0.64253(11) | 0.0447(9) |

values may indicate a higher Ca content than the refined one. Ideal BVS of 2.00 v.u. would be achieved assuming the site occupancies ($Mn_{0.75}Ca_{0.25}$) and ($Mn_{0.92}Ca_{0.08}$) at Mn(13) and Mn(15), respectively. Following Gagné and Hawthorne (2020), Mn(15) can be considered as a typical seven-fold coordinated site, because its bond distances are in the range 2.119–2.782 Å; in contrast, Mn(13), having the seventh ligand at 2.905 Å, may be more correctly considered as a six-fold coordinated site.

The largest Mn-centered polyhedron in the crystal structure of brattforsite is represented by the Mn(18) site. This position shows an eight-fold coordination, with < Mn–O > distance of 2.428 Å, comparable with the average distance of 2.420 Å reported by Moore and Araki (1979a) for the distorted cubic polyhedron surrounding the Mn(1) site of magnussonite. Mn(18) is a mixed (Mn,Ca) position, with BVS of 1.89 v.u.

Finally, there are two split cation positions, i.e., Mn(16) and Mn(21). The Mn(16) site is split into two sub-positions, Mn(16)a and Mg(16)b, having site occupancies $Mn_{0.93}$ and $Mg_{0.07}$, respectively. The former has a distorted square pyramidal coordination, with four O atoms forming the base and Cl occupying the pyramidal vertex. Assuming the full-occupancy of this position, the BVS is 1.91 v.u., agreeing with the occurrence of a divalent cation. Mg(16)b sub-site was refined using the scattering curve of Mg, owing to shorter bonds with ligands. It has a four-fold coordination with O atoms, at distances ranging between 1.94 and 2.27 Å. Two longer distances with Cl atoms (~ 3.28 and 3.42 Å) increase the coordination number to six, giving rise to a distorted octahedron. BVS at the Mg(16)b position is 1.84 v.u. Mn(21) is split into Mn(21)a and Mn(21)b. The coordination of Mn(21)a is similar to that observed for Mg(16)b, with four short bonds with O atoms, in the range 2.04–2.06 Å, and two long distances with Cl at 3.64 Å. Mn(21)b has a five-fold coordination, with four O atoms at distances in the range between 1.99 and 2.22 Å, and a Cl atom at 3.28 Å. BVS at these two sites are 1.91 and 1.84 v.u.

The oxygen atoms are usually four-fold coordinated, being bonded to three Mn sites and one As site. The O(4) and O(31) sites show three slightly different bonding configurations, owing to the split nature of the Mn(21) site. Three O sites have not a four-fold coordination: O(18) and O(23) are five-fold

**Table 5** Selected interatomic distances (in Å) for brattforsite

| | | | | | | | | |
|---|---|---|---|---|---|---|---|---|
| As(1) | – O(33) | 1.783(4) | As(2) | – O(12) | 1.763(4) | As(3) | – O(19) | 1.775(4) |
| | – O(34) | 1.787(4) | | – O(29) | 1.778(4) | | – O(32) | 1.778(4) |
| | – O(3) | 1.787(4) | | – O(8) | 1.785(4) | | – O(5) | 1.791(4) |
| | average | 1.786 | | average | 1.775 | | average | 1.781 |
| | BVS | 2.93 | | BVS | 3.00 | | BVS | 2.95 |
| As(4) | – O(17) | 1.785(4) | As(5) | – O(26) | 1.758(5) | As(6) | – O(10) | 1.748(4) |
| | – O(4) | 1.789(4) | | – O(20) | 1.800(4) | | – O(11) | 1.760(4) |
| | – O(27) | 1.805(4) | | – O(28) | 1.802(4) | | – O(31) | 1.785(4) |
| | average | 1.793 | | average | 1.787 | | average | 1.764 |
| | BVS | 2.88 | | BVS | 2.92 | | BVS | 3.08 |
| As(7) | – O(9) | 1.769(4) | As(8) | – O(35) | 1.772(4) | As(9) | – O(7) | 1.767(4) |
| | – O(30) | 1.774(4) | | – O(13) | 1.788(4) | | – O(18) | 1.769(4) |
| | – O(15) | 1.784(4) | | – O(14) | 1.791(4) | | – O(1) | 1.792(4) |
| | average | 1.776 | | average | 1.784 | | average | 1.776 |
| | BVS | 3.00 | | BVS | 2.94 | | BVS | 2.99 |
| As(10) | – O(16) | 1.758(4) | As(11) | – O(25) | 1.753(5) | As(12) | – O(21) | 1.766(4) |
| | – O(36) | 1.783(4) | | – O(23) | 1.757(4) | | – O(22) | 1.768(4) |
| | – O(2) | 1.793(4) | | – O(24) | 1.782(5) | | – O(6) | 1.788(4) |
| | average | 1.778 | | average | 1.764 | | average | 1.774 |
| | BVS | 2.98 | | BVS | 3.08 | | BVS | 3.01 |
| Mn(1) | – O(27) | 2.179(4) | Mn(2) | – O(9) | 2.072(4) | Mn(3) | – O(10) | 2.044(4) |
| | – O(27) | 2.179(4) | | – O(19) | 2.101(4) | | – O(12) | 2.070(4) |
| | – O(5) | 2.223(4) | | – O(32) | 2.268(4) | | – O(11) | 2.205(4) |
| | – O(5) | 2.223(4) | | – O(8) | 2.286(4) | | – O(15) | 2.253(4) |
| | – O(19) | 2.279(4) | | – O(29) | 2.323(4) | | – O(30) | 2.358(4) |
| | – O(19) | 2.279(4) | | – O(5) | 2.324(4) | | – O(31) | 2.386(4) |
| | average | 2.227 | | average | 2.229 | | average | 2.219 |
| | BVS | 1.89 | | BVS | 1.92 | | BVS | 2.00 |
| Mn(4) | – O(14) | 2.098(4) | Mn(5) | – O(5) | 2.099(4) | Mn(6) | – O(8) | 2.165(4) |
| | – O(30) | 2.174(4) | | – O(29) | 2.108(4) | | – O(2) | 2.203(4) |
| | – O(28) | 2.208(4) | | – O(18) | 2.206(4) | | – O(33) | 2.222(4) |
| | – O(24) | 2.233(5) | | – O(36) | 2.241(4) | | – O(19) | 2.225(4) |
| | – O(10) | 2.243(5) | | – O(3) | 2.355(4) | | – O(27) | 2.254(4) |
| | – O(22) | 2.327(4) | | – O(17) | 2.385(4) | | – O(7) | 2.263(4) |
| | average | 2.214 | | average | 2.232 | | average | 2.222 |
| | BVS | 1.95 | | BVS | 1.91 | | BVS | 1.89 |
| Mn(7) | – O(17) | 2.046(4) | Mn(8) | – O(31) | 2.137(4) | Mn(9) | – O(13) | 2.190(4) |
| | – O(23) | 2.070(4) | | – O(20) | 2.172(5) | | – O(32) | 2.209(4) |
| | – O(2) | 2.113(4) | | – O(1) | 2.179(4) | | – O(34) | 2.232(4) |
| | – O(27) | 2.174(4) | | – O(12) | 2.217(4) | | – O(9) | 2.242(4) |
| | – O(4) | 2.215(4) | | – O(4) | 2.230(4) | | – O(16) | 2.266(4) |
| | average | 2.124 | | – O(23) | 2.316(5) | | – O(6) | 2.267(4) |
| | BVS | 2.02 | | average | 2.208 | | average | 2.234 |
| Mn(10) | – O(22) | 2.114(4) | | BVS | 1.97 | | BVS | 1.88 |
| | – O(3) | 2.115(4) | Mn(11) | – O(26) | 1.996(4) | Mn(12) | – O(35) | 2.043(4) |
| | – O(1) | 2.144(4) | | – O(7) | 2.076(4) | | – O(16) | 2.084(4) |
| | – O(20) | 2.154(4) | | – O(6) | 2.154(4) | | – O(14) | 2.214(4) |
| | – O(28) | 2.219(4) | | – O(34) | 2.241(4) | | – O(13) | 2.303(4) |
| | – O(18) | 2.914(5) | | – O(33) | 2.296(4) | | – O(24) | 2.308(5) |
| | average | 2.277 | | average | 2.153 | | – O(25) | 2.657(6) |
| | BVS | 1.94 | | BVS | 1.92 | | average | 2.268 |
| Mn(13) | – O(24) | 2.153(4) | Mn(14) | – O(13) | 2.093(4) | | BVS | 1.87 |
| | – O(6) | 2.192(4) | | – O(13) | 2.093(4) | Mn(15) | – O(34) | 2.187(4) |
| | – O(2) | 2.264(4) | | – O(32) | 2.111(4) | | – O(15) | 2.206(4) |
| | – O(1) | 2.290(5) | | – O(32) | 2.111(4) | | – O(20) | 2.219(5) |
| | – O(7) | 2.329(4) | | – Cl(1) | 2.9386(17) | | – O(29) | 2.255(4) |
| | – O(16) | 2.366(4) | | – Cl(1) | 2.9386(17) | | – O(9) | 2.345(4) |
| | – O(23) | 2.905(5) | | average | 2.381 | | – O(12) | 2.437(5) |
| | average | 2.357 | | BVS | 1.90 | | – O(26) | 2.714(8) |
| | BVS | 1.81 | Mg(16)b | – O(33) | 1.94(3) | | average | 2.338 |
| Mn(16)a | – O(30) | 2.079(4) | | – O(30) | 1.98(3) | | BVS | 1.82 |

**Table 5** (continued)

| | | | | | | | | |
|---|---|---|---|---|---|---|---|---|
| | – O(8) | 2.097(4) | | – O(8) | 2.23(3) | Mn(17) | – O(21) | 2.110(4) |
| | – O(28) | 2.109(4) | | – O(28) | 2.27(3) | | – O(25) | 2.134(4) |
| | – O(33) | 2.113(4) | | average | 2.10 | | – O(15) | 2.138(4) |
| | – Cl(2) | 2.693(2) | | BVS | 1.77* | | – O(11) | 2.141(4) |
| | average | 2.218 | Mn(19) | – O(21) | 2.100(4) | | – O(35) | 2.287(4) |
| | BVS | 1.92* | | – O(36) | 2.154(4) | | – O(26) | 2.346(5) |
| Mn(18) | – O(11) | 2.302(5) | | – O(3) | 2.192 | | average | 2.193 |
| | – O(11) | 2.302(5) | | – O(22) | 2.385(5) | | BVS | 2.07 |
| | – O(14) | 2.323(4) | | – Cl(1) | 2.424(2) | Mn(20) | – O(25) | 2.160(6) |
| | – O(14) | 2.323(4) | | – O(18) | 2.565(4) | | – O(18) | 2.214(4) |
| | – O(35) | 2.447(4) | | average | 2.303 | | – O(36) | 2.303(4) |
| | – O(35) | 2.447(4) | | BVS | 1.92 | | – O(17) | 2.362(4) |
| | – O(10) | 2.642(5) | Mn(21)b | – O(31) | 1.990(6) | | – Cl(2) | 2.566(2) |
| | – O(10) | 2.642(5) | | – O(4) | 2.036(9) | | – O(23) | 2.748(5) |
| | average | 2.428 | | – O(31) | 2.092(17) | | average | 2.392 |
| | BVS | 1.87 | | – O(4) | 2.22(2) | | BVS | 1.92 |
| Mn(21)a | – O(31) | 2.039(4) | | – Cl(2) | 3.28(5) | | | |
| | – O(31) | 2.039(4) | | average | 2.32 | | | |
| | – O(4) | 2.057(4) | | BVS | 1.84* | | | |
| | – O(4) | 2.057(4) | | | | | | |
| | average | 2.048 | | | | | | |
| | BVS | 1.91* | | | | | | |

*BVS was calculated assuming full-occupancy of the site

coordinated, forming bonds with four Mn sites (one Mn–O distance being larger than 2.90 Å) and one As site, whereas O(21) has a three-fold coordination with two Mn and one As sites. BVS at the O sites range between 1.86 and 2.06 v.u., confirming the occurrence of $O^{2-}$ at these sites. Chlorine and minor (OH) groups are hosted at two sites, Cl(1) and Cl(2). These two sites are bonded to two Mn atoms, achieving a relatively low BVS of 0.55 and 0.65 v.u., respectively. Such an underbonding is related to the long Mn–Cl distances. Moore and Araki (1979a) found similar long distance in magnussonite, stressing that the observed distance is 0.30 Å longer than that predicted on the basis of ionic radii, i.e., 2.51 Å.

**Table 6** Bond valence sums (in valence units) for anion sites in brattforsite

| | | | | | |
|---|---|---|---|---|---|
| O(1) | 1.96 | O(13) | 2.01 | O(25) | 1.99 |
| O(2) | 1.98 | O(14) | 2.00 | O(26) | 1.91 |
| O(3) | 1.95 | O(15) | 1.99 | O(27) | 1.93 |
| O(4)* | 2.04<br>1.86<br>2.06 | O(16) | 1.99 | O(28) | 1.98 |
| O(5) | 1.95 | O(17) | 1.94 | O(29) | 1.95 |
| O(6) | 1.97 | O(18) | 1.92 | O(30) | 2.04 |
| O(7) | 2.00 | O(19) | 2.01 | O(31)* | 2.04<br>1.94<br>2.06 |
| O(8) | 2.02 | O(20) | 1.99 | O(32) | 2.02 |
| O(9) | 2.01 | O(21) | 1.86 | O(33) | 1.98 |
| O(10) | 1.98 | O(22) | 1.88 | O(34) | 1.93 |
| O(11) | 2.05 | O(23) | 1.92 | O(35) | 1.97 |
| O(12) | 1.99 | O(24) | 1.92 | O(36) | 1.96 |
| Cl(1) | 0.55 | Cl(2) | 0.65 | | |

* O(4) and O(31) are involved in three different bond configurations; the three BVS values refer to such configurations

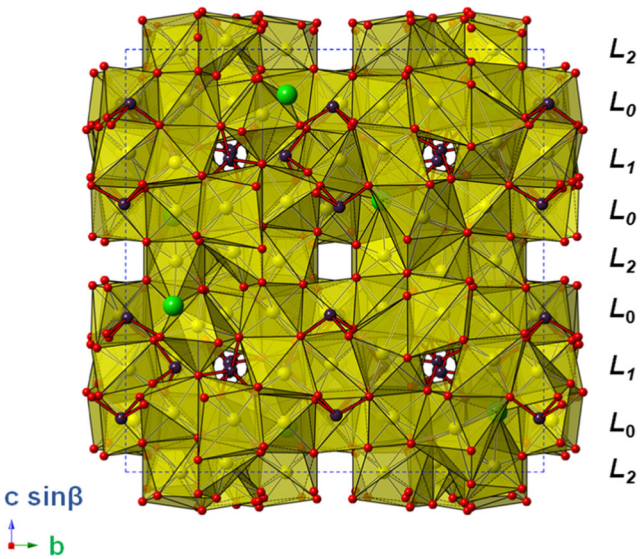


**Fig. 5** The crystal structure of brattforsite, as seen down *a*. Symbols: yellow polyhedra are Mn-centered sites. Circles: dark violet = As sites; green = Cl sites; red = O sites. As–O bonds are shown as red sticks. Unit-cell is shown by dashed lines. $L_0$, $L_1$, and $L_2$ indicate the structural layers shown in Fig. 7

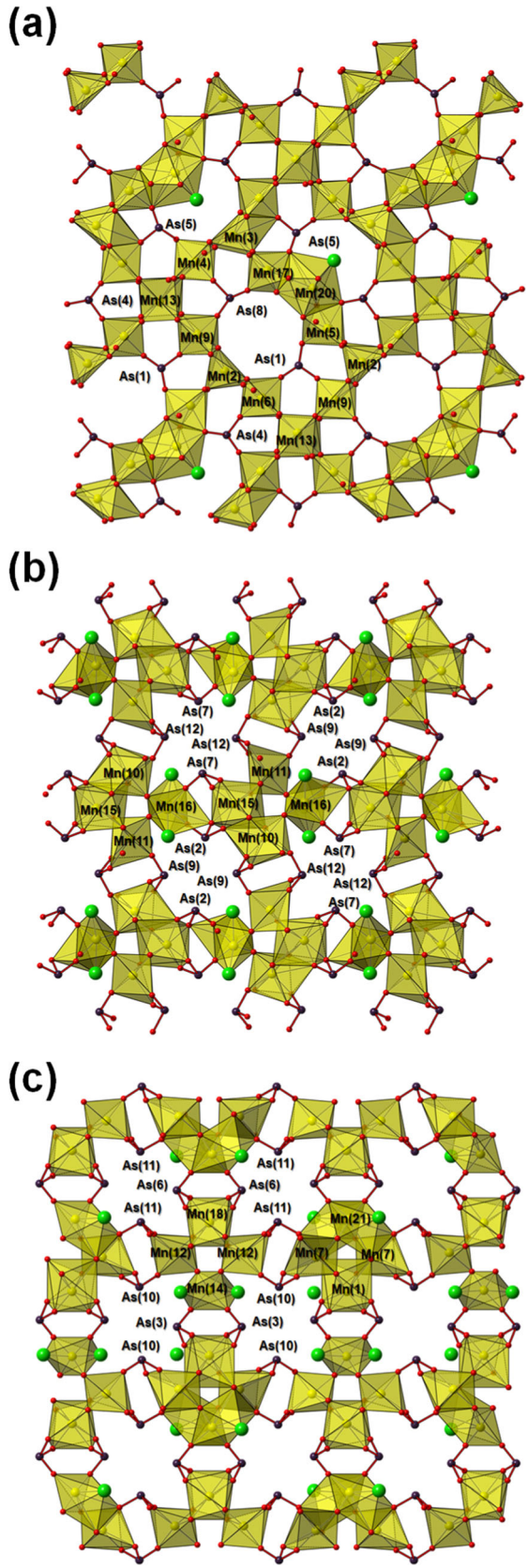


**Fig. 6** The polyhedral layers occurring in the crystal structure of brattforsite: $L_0$ (**a**), $L_1$ (**b**), and $L_2$ (**c**), as seen down *c* (*a* horizontal)

The structural formula derived through the crystal structure refinement of brattforsite is $(Mn_{18.24}Ca_{0.69}Mg_{0.07})_{\Sigma 19.00}(As^{3+}O_3)_{12}$ $[Cl_{1.89}(OH)_{0.11}]$ ($Z = 8$). The total site scattering refined at the Mn sites is 470.6 electrons per formula unit (epfu), to be compared with a calculated site scattering of 466.8 epfu derived from the chemical analysis after the normalization of Σ(Mn, Ca, Mg, Fe) = 19 *apfu*. The actual partitioning of Mg and Ca is not determined. It is likely that they could be disordered over several mixed (Mn, Ca, Mg) sites, with Ca preferentially ordered at the larger Mn positions and Mg within the smaller Mn polyhedra. The minor amount of Fe was not located either, owing to the similar scattering factor to Mn; taking into account the results of Hålenius and Lindqvist (1996) for the related mineral magnussonite, as well as the result of optical absorption spectroscopic measurements performed on brattforsite, Fe may be hosted in the four-fold coordination or in a strongly axially distorted octahedral coordination.

## Discussion

### Brattforsite and its relationships with magnussonite

Brattforsite is related to the manganese arsenite mineral magnussonite. The definition of this latter mineral has yet not been fully clarified. Its crystal structure was solved by Moore and Araki (1979a) in the cubic space group $Ia\bar{3}d$, with unit-cell parameter $a = 19.680(4)$ Å. The authors proposed the ideal formula $Mn^{2+}{}_{18}[As^{3+}{}_6Mn^{+}O_{18}]_2Cl_2$ ($Z = 8$) or $Mn_{20}As_{12}O_{32}Cl_2$. This was questioned by Dunn and Ramik (1984), who highlighted that their analyses of magnussonite, as well as those given by Gabrielson (1956), showed (OH) > Cl. Similar results were obtained by Hålenius and Lindqvist (1996). Despite the apparent cubic character of magnussonite, some details suggest that further studies are needed to fully characterize this mineral. For example, crystals are optically anisotropic and biaxial (–) in sufficiently thick sections (~ 0.1 mm), with a very small $2V$ and birefringence. In addition, the stability of the $Mn^{+}$ ion in Nature is questioned, and no features ascribed to this rare cationic species have observed in optical spectra of magnussonite (Hålenius and Lindqvist 1996). Finally, the role of minor elements (e.g., Cu) has to be clarified. Figure 7 compares the crystal structure of magnussonite with that of brattforsite. One feature common to both structures is an As-octahedron, with As–As distances of 3.64 Å in magnussonite (actually ranging between 3.56 and 3.71 Å) and 3.66 Å in brattforsite (ranging between 3.49 and 3.78 Å). This octahedron is occupied by $Mn^{1+}$ (at 0, 0, 0) in magnussonite (according to Moore and Araki 1979a), with <Mn–As> distance of 2.65 Å. In brattforsite, this position is empty, and the shortest Mn–As distance was observed

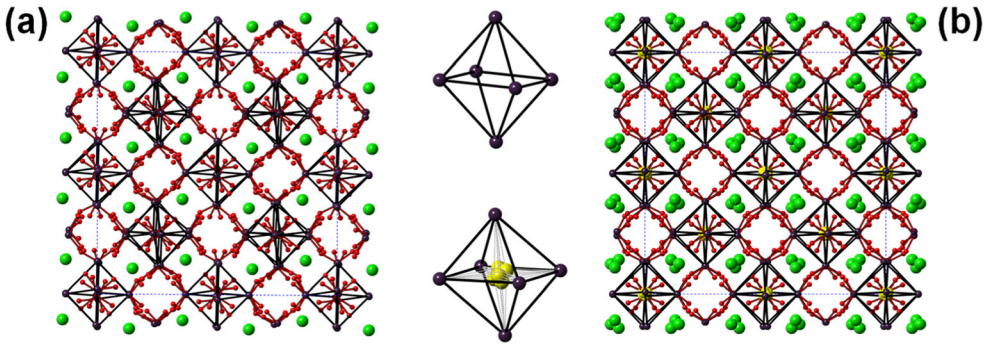


**Fig. 7** Projection of the crystal structure of brattforsite (**a**) and magnussonite (**b**) down *b* (*a* horizontal). Circles represent As (violet), Cl (green), and O (red) sites. In magnussonite, the Mn(5) site is shown as yellow circles. As–O bonds are shown as red thick lines, whereas As–As contacts are shown by thick black lines. In the center of the Fig., the As6-octahedra occurring in brattforsite (above) and magnussonite (below) are shown. In this latter image, Mn–As contacts are shown as dotted grey lines

between As(12) and Mn(19), with a distance of 2.9482(10) Å. No residuals were found in the difference-Fourier maps at coordinates (0, 0, 0). Neglecting minor differences in the cation coordinations, this is the main difference between brattforsite and magnussonite, which can be considered as having a homeotypic relationship. The spectroscopic data strengthen the picture of a close structural relationship between these two minerals, with, e.g., only small shifts in Raman bands (ca. 25 $cm^{-1}$) mainly related to the variation in overall < As–O > bond distances, 1.778 Å for brattforsite and 1.760 Å for magnussonite.

Consequently, based on structural details, the overall crystal symmetry, the chemical composition and the optical characteristics, brattforsite is distinct from magnussonite, and a *bona fide* Cl-analogue. At present there is no suggestion of the upper limit of Cl incorporation in magnussonite. Nysten (2003) identified a Cl-rich specimen (1.9 wt% Cl) from the Garpenberg Norra deposit, Dalecarlia, Sweden, with no indication of lower symmetry than cubic from single-crystal X-ray diffraction data.

## Brattforsite in the domain of Mn arsenite minerals

Currently, ca. 70 mineral species have Mn and As as essential chemical constituents. However, the large majority of these minerals has As in its pentavalent state, forming ($As^{5+}\phi_4$) oxyanions. Other phases have mixed ($As^{5+}\phi_4$) and ($As^{3+}\phi_3$) arrangements. Ten mineral species containing Mn and $As^{3+}$ are currently known; brattforsite is the eleventh mineral having species-defining Mn and $As^{3+}$. Table 7 lists these arsenite minerals.

Armangite is another example of fluorite-derivative structure (Moore and Araki 1979b), along with brattforsite and magnussonite. Its crystal structure is formed by a framework of Mn-centered polyhedra, with cavities lined by six ($AsO_3$) groups, which point their lone-electron-pairs into the center of

**Table 7** Currently known Mn arsenite minerals

| Mineral | Chemical formula* | *a* (Å) | *b* (Å) | *c* (Å) | α (°) | β (°) | γ (°) | s.g. | Ref. |
|---|---|---|---|---|---|---|---|---|---|
| Armangite | $Mn^{2+}_{26}[As^{3+}_{6}(OH)_4O_{14}][As^{3+}_{6}O_{18}]_2(CO_3)$ | 13.49 | 13.49 | 8.86 | 90 | 90 | 120 | $P\bar{3}$ | [1] |
| Brattforsite | $Mn_{19}As_{12}O_{36}Cl_2$ | 19.58 | 19.58 | 19.76 | 90 | 90.4 | 90 | $I2a$ | [2] |
| Cuyaite | $Ca_2Mn^{3+}As^{3+}_{14}O_{24}Cl$ | 14.72 | 5.59 | 17.42 | 90 | 112.4 | 90 | $Pn$ | [3] |
| Lepageite | $Mn^{2+}_{3}(Fe^{3+}_{7}Fe^{2+}_{4})O_3[Sb^{3+}_{5}As^{3+}_{8}O_{34}]$ | 10.61 | 10.44 | 15.26 | 89.6 | 104.5 | 89.7 | $P\bar{1}$ | [4] |
| Magnussonite | $Mn^{2+}_{10}As^{3+}_{6}O_{18}(OH,Cl)$ | 19.68 | 19.68 | 19.68 | 90 | 90 | 90 | $Ia\bar{3}\,d$ | [5] |
| Manganarsite | $Mn^{2+}_{3}As^{3+}_{2}O_4(OH)_4$ | 11.45 | 11.45 | 7.25 | 90 | 90 | 120 | $P\bar{3}\,1m$, $P31m$, or $P312$ | [6] |
| Nelenite | $Mn^{2+}_{16}As^{3+}_{3}Si_{12}O_{36}(OH)_{17}$ | 23.24 | 13.42 | 7.38 | 90 | 105.2 | 90 | $C2/m$ | [7] |
| Rouseite | $Pb_2Mn^{2+}(AsO_3)_2{\cdot}2H_2O$ | 6.36 | 7.29 | 5.54 | 97.3 | 114.2 | 106.0 | $P\bar{1}$ or $P1$ | [8] |
| Schallerite | $Mn^{2+}_{16}As^{3+}_{3}Si_{12}O_{36}(OH)_{17}$ | 13.42 | 13.42 | 14.32 | 90 | 90 | 120 | $P6_3$ | [9] |
| Trigonite | $Pb_3Mn^{2+}(AsO_3)_2(AsO_2OH)$ | 7.26 | 6.78 | 11.09 | 90 | 91.5 | 90 | $Pn$ | [10] |
| Wiklundite | $Pb_2(Mn^{2+},Zn)_3(Fe^{3+},Mn^{2+})_2(Mn^{2+},Mg)_{19}(As^{3+}O_3)_2[(Si,As^{5+})O_4]_6(OH)_{18}Cl_6$ | 8.26 | 8.26 | 126.59 | 90 | 90 | 120 | $R\bar{3}\,c$ | [11] |

*Chemical formulae after the official IMA-CNMNC List of Mineral Names (updated November 2020). s.g. = space group. References: [1] Moore and Araki (1979b); [2] this work; [3] Kampf et al. (2020); [4] Pieczka et al. (2019); [5] Moore and Araki (1979a); [6] Peacor et al. (1986); [7] Dunn and Peacor (1984); [8] Dunn et al. (1986); [9] Kato and Watanabe (1992); [10] Pertlik (1978); [11] Cooper et al. (2017)

such cavities, similarly to what is observed in brattforsite. Along with nelenite, schallerite, and trigonite, armangite is characterized by the occurrence of $[As^{3+}O_2(OH)]$ groups, together with $(AsO_3)$ groups. Nelenite and schallerite are dimorphs of the compound $Mn^{2+}{}_{16}As^{3+}{}_3Si_{12}O_{36}(OH)_{17}$. Whereas the crystal structure of the latter was solved by Kato and Watanabe (1992), the crystal structure of nelenite is still unknown, although Dunn and Peacor (1984) proposed a relation with friedelite. Both are T-O phyllosilicates, with $(AsO_3)$ groups hosting at partially occupied positions, and residing within large twelve-membered rings.

Manganarsite is another mineral related to schallerite. Also in this case the crystal structure is only hypothetical, and Peacor et al. (1986) proposed the occurrence of rings or chains of $(AsO_3)$ groups. Trigonite displays an open heteropolyhedral network, with (010) heteropolyhedral sheets cross-linked by additional $(As\phi_3)$ groups; the large cavities of this framework host $Pb^{2+}$ cations (Pertlik 1978). Dunn et al. (1986) proposed that trigonite is structurally related to rouseite, whose crystal structure is currently unknown. It is worth noting that all these minerals have their type localities at Långban-type ore deposits (i.e., Långban and Nordmark, in Sweden), or at Franklin-Sterling Hill-type deposits (in USA). Another mineral found in the same kind of occurrence (Långban) is wiklundite, a mineral representing a transition towards the mixed $As^{3+}$-$As^{5+}$ species (Cooper et al. 2017). Indeed, $As^{5+}$ occurs only as a minor substituent of $Si^{4+}$ and consequently only $As^{3+}$ can be considered as species-defining. Its complex layered crystal structure is characterized by the presence of isolated $(AsO_3)$ groups. Like brattforsite, wiklundite contains Mn and Cl as species-defining elements. An additional example is the recently described mineral cuyaite (Kampf et al. 2020), although with a different Mn valency (3+ instead of 2+). Its crystal structure can be described as an arsenite framework, with $(AsO_3)$ groups sharing corners. In contrast, brattforsite can be considered as a Mn-polyhedral framework. It is worth noting that Cl in cuyaite is severely underbonded (only 0.26 v.u.), and Kampf et al. (2020) attributed this discrepancy to the inability of the bond-valence theory to take the effect of the lone-electron-pair in account. In fact, Cl is hosted at the centre of channels accommodating the lone-electron-pairs of As sites. The underbonding of the Cl sites in brattforsite cannot be explained in this a way, since the lone-electron-pairs of the $As^{3+}$ sites do not point towards Cl atoms. Cuyaite is one of the two manganese arsenites not found in Långban-type occurrences, with the type locality in the Camarones Valley, Chile. The other one is lepageite, discovered in the Szklary pegmatite, Poland (Pieczka et al. 2019). Its crystal structure is characterized by a finite $[Sb_4As_4O_{19}]$ cluster and by isolated $(AsO_3)$ groups.

Manganese arsenites are apparently very rare in Nature, with reduced mineral assemblages of Långban or Franklin-Sterling Hill types of deposits representing their preferred kind of occurrence. Brattforsite, showing a close relationship with magnussonite and some structural similarity with armangite, is thus an interesting new addition to this category of minerals. In terms of mineral classification, it belongs to the Strunz group 4.JB, i.e., Arsenites, antimonites, bismuthites, with additional anions, without $H_2O$ (Strunz and Nickel 2001).

**Supplementary Information** The online version contains supplementary material available at https://doi.org/10.1007/s00710-021-00749-9.

**Acknowledgements** Torbjörn Lorin helped with colour photography of the type specimen. The paper benefited from reviews made by Adam Pieczka and an anonymous referee, and suggestions from the journal editor Maarten A.T.M. Broekmans.

**Funding** Open access funding provided by Swedish Museum of Natural History.



## References

Bernardini S, Bellatreccia F, Della Ventura G, Sodo A (2021) A reliable method for determining the oxidation state of manganese at the microscale in Mn oxides via Raman spectroscopy. Geostand Geoanal Res 45:223–244

Björck L (1986) Beskrivning till Berggrundskartan Filipstad NV. Sverig Geolog Undersök Af 147:1–110

Boström K, Rydell H, Joensuu O (1979) Långban - An exhalative sedimentary deposit? Econ Geol 74:1002–1011

Brese NS, O'Keeffe M (1991) Bond-valence parameters for solids. Acta Crystallogr B 47:192–197

Bruker AXS, Inc. (2016) APEX 3. Bruker Advanced X-ray Solutions, Madison

Christy AG, Gatedal K (2005) Extremely Pb-rich rock-forming silicates including a beryllian scapolite and associated minerals in a skarn from Långban, Värmland, Sweden. Mineral Mag 69:995–1018

Cooper MA, Hawthorne FC, Langhof J, Hålenius U, Holtstam D (2017) Wiklundite, ideally $Pb_2{}^{[4]}(Mn^{2+},Zn)_3(Fe^{3+},Mn^{2+})_2(Mn^{2+},Mg)_{19}(As^{3+}O_3)_2[(Si,As^{5+})O_4]_6(OH)_{18}Cl_6$, a new mineral from Långban, Värmland, Sweden: Description and crystal structure. Mineral Mag 81:841–855

Cooper MA, Raade G, Ball NA, Abdu YA, Hawthorne FC, Rowe R (2018) Folvikite, $Sb^{5+}Mn^{3+}(Mg,Mn^{2+})_{10}O_8(BO_3)_4$, a new oxyborate mineral from the Kitteln mine, Nordmark ore district, Värmland, Sweden: description and crystal structure. Mineral Mag 82:821–836

Dunn PJ, Peacor DR (1984) Nelenite, a manganese arsenosilicate of the friedelite group, polymorphous with schallerite, from Franklin, New Jersey. Mineral Mag 48:271–227

Dunn PJ, Peacor DR, Sturman BD, Wicks FJ (1986) Rouseite, a new lead manganese arsenite from Långban, Sweden. Am Mineral 71:1034–1036

Flink G (1917) Einige Neuigkeiten in schwedischer Mineralogie. Katoptrit, ein neues Mineral vor Nordmarken. Geol Foren Stock For 40:426–452

Frost RL, Bahfenne S (2010) Raman spectroscopic study of the arsenite minerals leiteite $ZnAs_2O_4$, reinerite $Zn_3(AsO_3)_2$ and cafarsite $Ca_5(Ti, Fe, Mn)_7(AsO_3)_{12}\cdot 4H_2O$. J Raman Spectrosc 41:325–328

Gabrielson O (1956) Magnussonite, a new arsenite mineral from the Långban mine in Sweden. Ark Min Geol 2:133–135

Gagné OC, Hawthorne FC (2015) Comprehensive derivation of bond-valence parameters for ion pairs involving oxygen. Acta Crystallogr B 71:562–578

Gagné OC, Hawthorne FC (2020) Bond-length distributions for ions bonded to oxygen: results for the transition metals and quantification of the factors underlying bond-length variation in inorganic solids. IUCrJ 7:581–629

Hålenius U, Lindqvist B (1996) Chromophoric divalent iron in optically anisotropic magnussonite. Eur J Mineral 5:25–34

Holtstam D, Langhof J (1995) Metamorphic harkerite from Nordmarks odalfält. Värmland Sweden GFF 117:151–152

Holtstam D, Mansfeld J (2001) Origin of a carbonate-hosted Fe-Mn-(Ba-As-Pb-Sb-W) deposit of Långban-type in Central Sweden. Miner Deposita 36:641–657

Holtstam D, Nysten P, Gatedal K (1998) Parageneses and compositional variations of Sb oxyminerals from Långban-type deposits in Värmland, Sweden. Mineral Mag 62:395–407

Kampf AR, Mills SJ, Nash B, Dini M, Donoso AAM (2020) Cuyaite, $Ca_2Mn^{3+}As^{3+}{}_{14}O_{24}Cl$, a new mineral with an arsenite framework from near Cuya, Camarones Valley, Chile. Mineral Mag 84:477–484

Kato T, Watanabe I (1992) The crystal structure of schallerite and friedelite. Yamaguchi University, College of Arts Bulletin 26:51–63

Magnusson NH (1929) Nordmarks malmtrakt. Sverig Geol Undersök Ca 13:1–98

Majzlan J, Drahota P, Filippi M (2014) Parageneses and crystal chemistry of arsenic minerals. Rev Mineral Geochem 79:17–184

Mandarino J (1981) The Gladstone-Dale relationship: part IV. The compatibility concept and its application. Can Mineral 19:441–450

Mighell AD (2003) Conventional cells: monoclinic *I*- and *C*-centered cells. Acta Crystallogr B59:300–302

Moore PB (1970a) Stenhuggarite, a new mineral from Långban and new data on magnussonite. Ark Min Geol 5:55–62

Moore PB (1970b) Mineralogy and chemistry of Långban-type deposits in Bergslagen, Sweden. Mineral Rec 1:154–172

Moore PB (1978) Manganhumite, a new species. Mineral Mag 42:133–136

Moore PB, Araki T (1979a) Magnussonite, manganese arsenite, a fluorite derivative structure. Am Mineral 64:390–401

Moore PB, Araki T (1979b) Armangite, $Mn^{2+}{}_{26}[As^{3+}{}_6(OH)_4O_{14}][As^{3+}{}_6O_{18}]_2[CO_3]$, a fluorite derivative structure. Am Mineral 64:748–757

Nysten P (2003) Yeatmanite and magnussonite from the Garpenberg Norra mine, Bergslagen ore province, Sweden. Can Mineral 41:201–206

Nysten P, Holtstam D, Jonsson E (1999) The Långban minerals. In: Holtstam D, Langhof J (eds) Långban: the mines, their minerals, geology and explorers. Naturhistoriska riksmuseet and Raster Förlag, Stockholm

Pasero M (2021) The new IMA list of minerals – A work in progress – Updated: March 2021. http://cnmnc.main.jp/IMA_Master_List_%282021-03%29.pdf

Peacor DR, Dunn PJ, Simmons WB, Wicks FJ (1986) Arsenites related to layer silicates: Manganarsite, the arsenite analogue of manganpyrosmalite, and unnamed analogues of friedelite and schallerite from Långban, Sweden. Am Mineral 71:1517–1521

Pertlik F (1978) The crystal structure of trigonite, $Pb_3Mn(AsO_3)_2(AsO_2OH)$. Tscher Miner Petrog 25:95–105

Pieczka A, Cooper MA, Hawthorne FC (2019) Lepageite, $Mn^{2+}{}_3(Fe^{3+}{}_7Fe^{2+}{}_4)O_3[Sb^{3+}{}_5As^{3+}{}_8O_{34}]$, a new arsenite-antimonite mineral from the Szklary pegmatite, Lower Silesia, Poland. Am Mineral 104:1043–1050

Pouchou JL, Pichoir F (1984) A new model for quantitative X-ray microanalysis. I. Application to the analysis of homogeneous samples. Rech Aerospatiale 3:13–36

Sandström F, Holtstam D (1999) Geology of the Långban deposit. In: Holtstam D, Langhof J (eds) Långban: the mines, their minerals, geology and explorers. Naturhistoriska riksmuseet and Raster Förlag, Stockholm

Sheldrick GM (2015) Crystal structure refinement with SHELXL. Acta Crystallogr C71:3–8

Sjögren H (1884) Om manganarseniaternas från Nordmarken förekomstsätt och paragenesis. Geol Foren Stock For 7:407–416

Smith DGW, Nickel EH (2007) A system for codification for unnamed minerals: report of the subcommittee for unnamed minerals of the IMA Commission on New Minerals. Nomenclature Classification Can Mineral 45:983–1055

Stephens MB, Ripa M, Lundström I, Persson L, Bergman T, Ahl M, Wahlgren CH, Persson PO, Wickström L (2009) Synthesis of the bedrock geology in the Bergslagen region, Fennoscandian Shield, south-central Sweden. Sverig Geol Undersök Rapp Med Ba 58:1–259

Strunz H, Nickel E (2001) Strunz Mineralogical Tables. Chemical-Structural Mineral Classification system. E. Schweizerbart'sche Verlagsbuchhandlung, Stuttgart

Wilson AJC (ed) (1992) International Tables for Crystallography, Volume C: Mathematical, physical and chemical tables. Kluwer Academic, Dordrecht